

Optimization of Electron Transport Layer-Free $\text{Cs}_2\text{TiBr}_6/\text{MASnBr}_3$ Laminated Structure Perovskite Solar Cells by SCAPS-1D Simulation

Ling You, Xin Zhang,* Qian Ma, Wu Zhu, and Jiang Wu

Cs_2TiBr_6 materials have promising applications in organic–inorganic halide perovskite solar cells (PSCs), but their power conversion efficiency (PCE) is low. Herein, based on the matching band structure of MASnBr_3 and Cs_2TiBr_6 , a no-electron transport layer (ETL)-structured laminated PSC is constructed for numerical simulation using SCAPS-1D. The results have shown that the ETL-free structure reduces the potential barrier between the interfaces and improves the performance of the device. MASnBr_3 is used to replace the traditional hole transport layer to form a laminated structure, which is more conducive to the built-in electric field of the device. Through exploring the internal influencing factors and applicable environment, it is found that the device can maintain a good operating level between 230 and 430 K. Finally, the best PCE of 19.63% is achieved in the proposed device structure ($\text{FTO}/\text{Cs}_2\text{TiBr}_6/\text{MASnBr}_3/\text{Au}$). This work provides a new approach to achieving lead-free and efficient laminated PSCs in a wide temperature range of usage environments from -43 to 157°C .

1. Introduction

Climate change is a major global challenge facing human beings today. Countries around the world have adopted a global agreement to reduce greenhouse gas emissions and thus put forward carbon peaking and carbon neutrality goals.^[1,2] As a new generation of clean energy, solar energy has a very broad development prospect. Organic–inorganic halide perovskite solar cells (PSCs) have rapidly developed as the leader in the new generation of batteries, and their power conversion efficiency (PCE) has increased from 3.8% to 25.6% in the last few years.^[3,4]

For PSCs, Pb in the perovskite absorber layer is often used as an element to ensure good optoelectronic properties of the device.^[5–9] However, the toxicity of lead is still the main obstacle to the industrialization of PSCs. Lead is a cumulative poison that


is difficult to excrete from the body, and it is also difficult to eliminate the harm of lead toxicity to the environment.^[10,11] In order to solve the toxicity problem of Pb^{2+} , a lot of research work has used environmentally friendly elements such as Sn^{2+} from this group to replace Pb^{2+} . Sn-based perovskite has good optoelectronic properties, and the device performance is ideal.^[12,13] However, the oxidation of Sn^{2+} to Sn^{4+} is a very spontaneous process, resulting in the self-doping phenomenon in the crystal, which leads to the degradation of device performance. Therefore, it is necessary to explore more stable and efficient alternative materials for lead-free perovskites. The study found that cesium-based lead-free halide perovskites are a favorable choice.^[14] Slavney et al. introduced Bi^{3+} into perovskite, making $\text{Cs}_2\text{AgBiBr}_6$ significantly

more stable than MAPbI_3 .^[15] Further, as a light element with abundant yield, nontoxicity, good stability, and good biocompatibility in the earth, Ti has been introduced to everyone's attention.^[16,17] Ju et al. proposed the potential of Ti-based PSCs in the photovoltaic field through theoretical calculations.^[18] Chen et al. prepared Cs_2TiBr_6 as the absorber layer of PSCs for the first time by the low-temperature steam method, and its PCE reached 3.3%.^[16] By preparing titanium-based perovskite materials, Kong et al. found that they have tunable bandgaps (1.38–1.78 eV) suitable for PSC applications.^[19] All of the above indicate that Cs_2TiBr_6 has broad application prospects in the field of PSC.

Further, in order for PSCs to meet the requirements of commercialization, reducing the preparation process and reducing the material cost are issues that cannot be ignored. The electron transport layer (ETL) in the traditional PSCs structure is removed to reduce the preparation process. Meanwhile, introducing a new absorber layer material instead of the hole transport layer (HTL) and allowing the device to form the laminated structure is an effective solution. Yang et al. used MAPbI_3 instead of the transport layer in PSCs to construct the $\text{MAPbI}_3/\text{FAPbI}_3$ laminated structure by the dynamic dropping technique,^[20] which enhanced the built-in electric field of PSCs and improved carrier transport in the device. He et al. constructed a $\text{CsPbBr}_3/\text{MAPbBr}_3$ laminated structure heterostructure, enabling PSCs to exhibit a PCE of 5.90%.^[21] Hao et al. introduced the tin-based perovskite material to make the device form lead–tin laminated structure.^[22] The built-in electric field generated enhanced the light absorption characteristics of the device, significantly

L. You, W. Zhu
College of Electronics and Information Engineering
Shanghai University of Electric Power
No. 2103 Pingliang Road, Shanghai 200090, China

X. Zhang, Q. Ma, J. Wu
College of Energy and Mechanical Engineering
Shanghai University of Electric Power
No. 2103 Pingliang Road, Shanghai 200090, China
E-mail: 397508968@qq.com

 The ORCID identification number(s) for the author(s) of this article can be found under <https://doi.org/10.1002/pssa.202300071>.

DOI: 10.1002/pssa.202300071

improving its performance while reducing the toxicity of lead. Therefore, using MASnBr_3 material to replace the expensive HTL, it is a good choice to make the device form a laminated structure to optimize the built-in electric field. However, in the existing reports, there are few studies on titanium-based PSCs, nor the effect of laminated structure on titanium-based PSCs.

Therefore, in this work, we constructed an ETL-free Cs_2TiBr_6 / MASnBr_3 laminated structure PSC and performed numerical simulations using SCAPS-1D. SCAPS-1D is a numerical simulation software for various thin films and PSCs. The effects of ETL-free structures and laminated structures on PSCs were explored. Using different materials, metal electrodes suitable for titanium-based PSCs were identified. The internal influencing factors of Ti-based PSCs without ETL structure were comprehensively investigated. It provides theoretical guidance for researchers to realize high-performance and low-cost Ti-based PSCs in the future.

2. Device Simulation and Model Verification

This study is based on SCAPS-1D software,^[23] which is widely used in the simulation of solar cells. Kumar et al. compared

$\text{CH}_3\text{NH}_3\text{PbI}_3$ and lead-free $\text{CH}_3\text{NH}_3\text{SnI}_3$ PSCs using SCAPS.^[24] Raj et al. performed numerical simulations on double-perovskite $\text{La}_2\text{NiMnO}_6$ PSCs, and the final optimized results exhibited an excellent PCE of 26.79%.^[25] As shown in Figure 1a, the structure of the device is glass/FTO/ Cs_2TiBr_6 / MASnBr_3 /Au, which is different from the n-i-p structure of conventional PSCs, which has no ETL. At the same time, MASnBr_3 is used to replace the traditional HTL to form a laminated structure, which is more conducive to the

Table 2. Interface defect parameters.

Parameter	ETL/Absorber	Absorber/HTL
Defect type	Neutral	Neutral
Capture cross section for electron [cm^2]	10^{-19}	10^{-18}
Capture cross section for hole [cm^2]	10^{-18}	10^{-19}
Energetic distribution	Single	Single
Energy level with respect to EV [eV]	0.6	0.6
Characteristic energy [eV]	0.1	0.1
Total density [cm^{-3}]	10^{13}	10^{13}

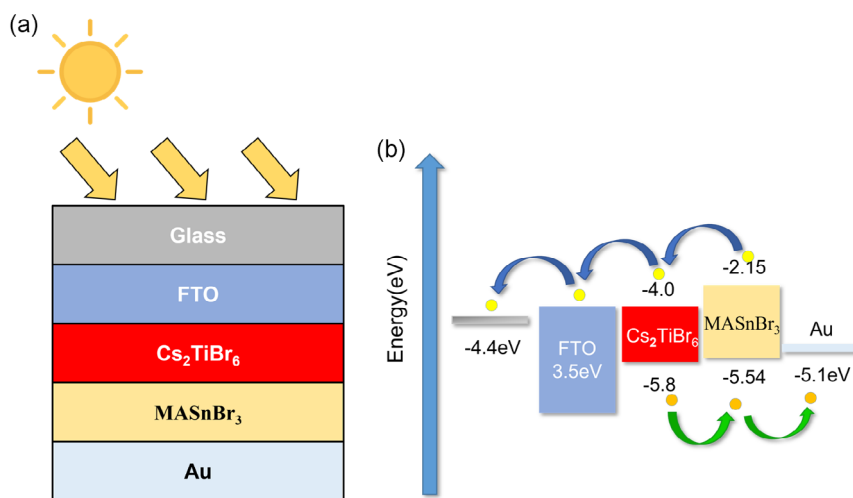


Figure 1. a) Schematic structure of a PSC. b) Energy band structure.

Table 1. Basic parameters of each layer of the device.

Parameter	FTO	TiO_2	Cs_2TiBr_6	MASnBr_3
Thickness [nm]	500	30	150	30
Bandgap, E_g [eV]	3.5	3.2	1.8	3.4
Electron affinity, χ [eV]	4	4.1	4	1.9
Dielectric permittivity, ϵ_r	9	9	10	10
CB effective density of states, N_c [cm^{-3}]	2.20×10^{18}	2.2×10^{18}	6.0×10^{19}	1.7×10^{19}
VB effective density of states, N_v [cm^{-3}]	1.80×10^{19}	1.0×10^{19}	2.14×10^{19}	2.5×10^{21}
Electron mobility, μ_n [$\text{cm}^2 \text{V}^{-1} \text{s}^{-1}$]	20	20	0.236	0.0001
Hole mobility, μ_p [$\text{cm}^2 \text{V}^{-1} \text{s}^{-1}$]	10	10	0.171	0.1
Shallow donor density, N_D [cm^{-3}]	1.0×10^{19}	1.0×10^{18}	3.0×10^{19}	0
Shallow acceptor density, N_A [cm^{-3}]	0	0	3.0×10^{18}	1.0×10^{18}
Defect density, N_t [cm^{-3}]	1.00×10^{14}	1.0×10^{15}	4.17×10^{15}	1.0×10^{15}

built-in electric field of the device. As shown in Figure 1b, the absorber layer Cs_2TiBr_6 is in direct contact with the FTO to transport the carriers.

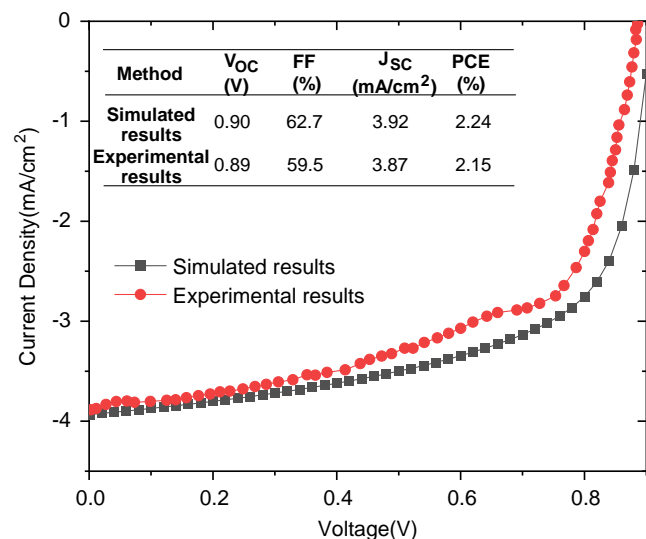


Figure 2. Comparison of simulation results with experimental results of J - V curves.

Through the latest reports of Ti-based PSCs experiments and simulations, the basic parameters of this structural material are listed in Table 1.^[26–29] Where E_g is band energy, χ is electron affinity, N_c and N_v are the effective densities of conduction band and valence band states, respectively, and N_t is the defect density. As shown in Table 2, it is the defect parameter between the absorption layer and the transmission layer. When the effect of temperature is not discussed, the operating temperature of the PSCs is 300 K. To verify the rationality of the initial parameter selection, we study initial Ti-based PSCs (FTO/ TiO_2 / Cs_2TiBr_6 / P_3HT /Au) with ETLs. By comparing the simulation results with the experimental results,^[16] as shown in Figure 2, it is found that the simulation results are in good agreement with the experimental results, which proves the rationality of the device.

3. Results and Discussion

3.1. The Effect of the ETL-free Structure on PSCs

In traditional PSCs, n - i - p is the most common structure, n is the ETL, which is used to exchange electrons with the absorption layer, and p is the HTL, which is used to exchange holes with the absorption layer, so as to ensure PSCs have good properties, and the ETL is often an indispensable part. However, the commonly used ETL (TiO_2) requires high-temperature calcination,

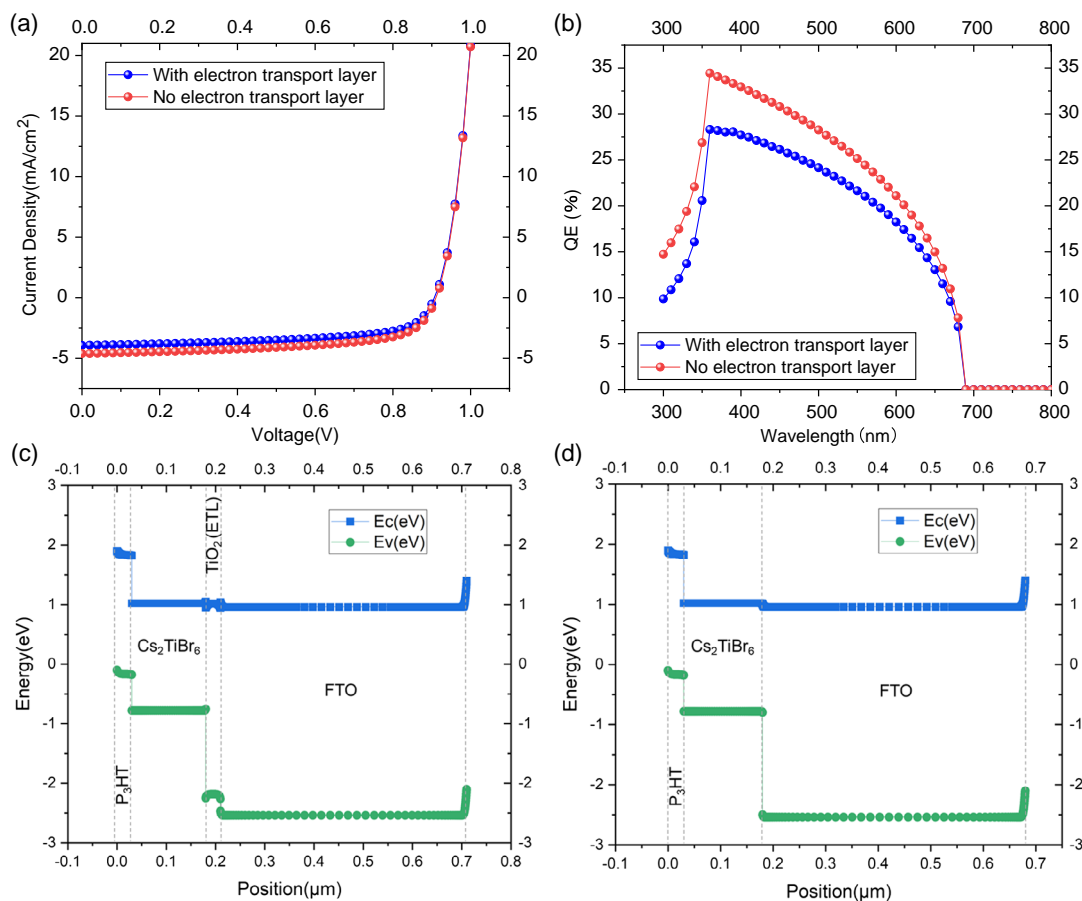


Figure 3. Influence of ETL structure on a) J - V and b) QE. c) With ETL energy band structure. d) No ETL energy band structure.

which increases the fabrication process of PSCs. At the same time, the direct contact of TiO_2 with the absorber layer will promote the decomposition of the perovskite absorber layer. Therefore, it is necessary to explore the effect of ETL structure on PSCs.

Table 3. Comparison with and without ETL.

Structures	V_{OC} [V]	J_{SC} [mA cm^{-2}]	FF [%]	PCE [%]
No ETL structure	0.91	4.61	62.5	2.63
With ETL structure	0.90	3.92	62.7	2.24

Table 4. Basic parameters of different ETL materials.

Parameters	P_3HT	MoO_3	Cu_2O	MASnBr_3	CuSCN	CuI
Thickness [nm]	30	30	30	30	30	30
Bandgap, E_g [eV]	2	3	2.17	2.15	3.4	2.98
Electron affinity, χ [eV]	3.2	2.5	3.2	3.39	1.9	2.1
Dielectric Permittivity, ϵ_r	3	12.5	6.6	8.2	10	6.5
CB effective density of states, N_c [cm^{-3}]	1.0×10^{20}	2.2×10^{18}	2.5×10^{20}	1.0×10^{18}	1.7×10^{19}	2.8×10^{19}
VB effective density of states, N_v [cm^{-3}]	1.0×10^{20}	1.8×10^{18}	2.5×10^{20}	1.0×10^{18}	2.5×10^{21}	1.0×10^{19}
Electron mobility, μ_n [$\text{cm}^2 \text{V}^{-1} \text{s}^{-1}$]	0.0001	25	80	1.6	0.0001	0.00017
Hole mobility, μ_p [$\text{cm}^2 \text{V}^{-1} \text{s}^{-1}$]	0.0001	100	80	1.6	0.1	0.0002
Shallow Acceptor density, N_A [cm^{-3}]	1.0×10^{17}	1.00×10^{18}	1.0×10^{18}	1.0×10^{18}	1.0×10^{18}	1.0×10^{18}
Defect density, N_t [cm^{-3}]	1.0×10^{17}	1.00×10^{15}	1.0×10^{15}	1.0×10^{15}	1.0×10^{15}	1.0×10^{15}

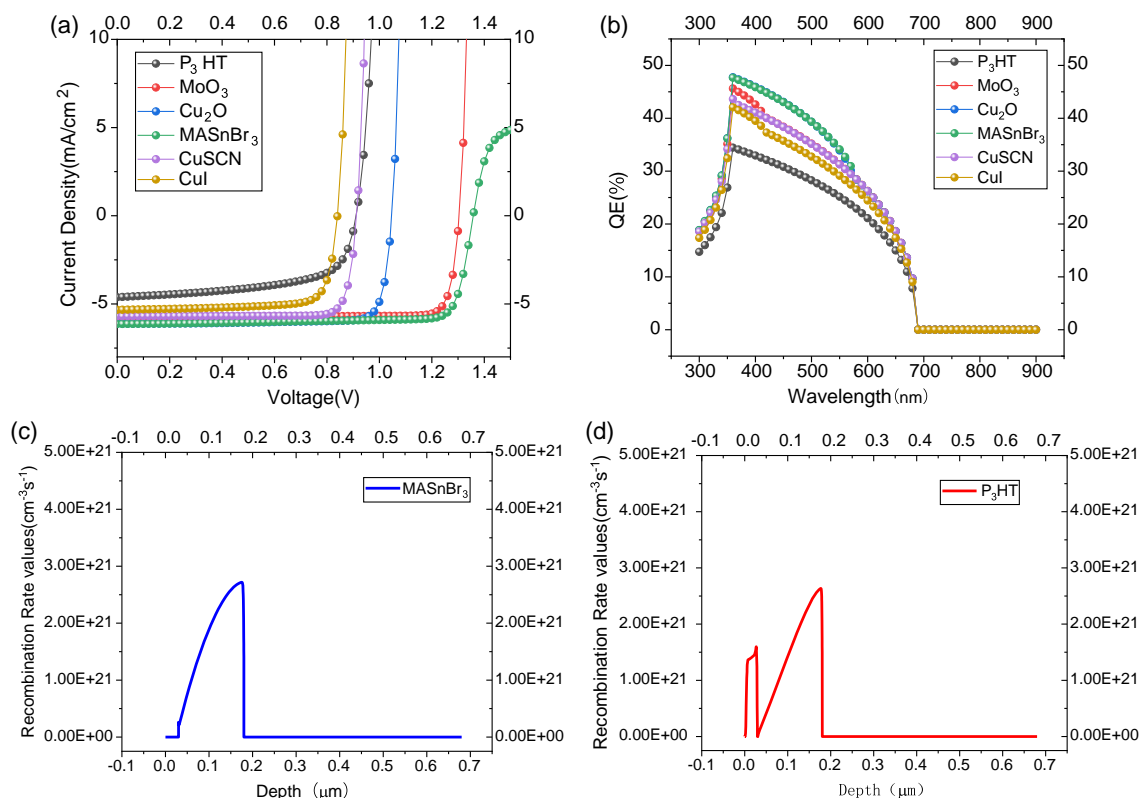


Figure 4. a) J - V curves of different ETLs and b) QE curves of different ETLs. Recombination rate: c) MASnBr_3 , d) P_3HT .

promoting the separation of carriers. To explore the reason for this phenomenon, the band structures of PSCs with and without ETLs were investigated. As illustrated in Figure 3c,d, when an ETL is included in the structure, a potential barrier is formed between the absorber layer/ETL and ETL/FTO, which hinders the transport of carriers. When the ETL is removed, the potential barrier between the absorber layer/ETL and ETL/FTO disappears, which improves the performance of the device. As shown in Table 3, after removing the ETL, the performance of the device improved from 2.24% to 2.63%. Therefore, FTO/Cs₂TiBr₆/P₃HT/Au was used as the basic structure of PSCs in the following research.

3.2. Influence of Laminated Structure Instead of HTL on Device Performance

In order to explore the effect of replacing the HTL with the laminated structure on the device performance, the performances of P₃HT, MoO₃, Cu₂O, CuSCN, and CuI as the HTL of the device and MASnBr₃ instead of the ETL structure were investigated. Table 4 shows the parameters of the ETL.^[30–35] As illustrated in Figure 4a, when MASnBr₃ is used instead of the HTL, the *J*–*V* curve is on the far right, indicating that the PSC with this structure has the best performance. When P₃HT and MnO₃ are used as the HTL, the *J*–*V* curve is on the left, meaning that the performance of the PSCs is poor at this time. Figure 4b also verifies this conclusion. When MASnBr₃ is used as a laminated

structure, the external quantum efficiency (QE) of the device is 360–490 nm, all above 40%. When P₃HT is used as HTL, the external QE of the device is only about 30% at 360–490 nm. This may be due to the fact that the construction of the laminated structure improves the built-in electric field of PSCs, which enhances the light absorption characteristics of the device.^[36] To explore the internal influence mechanism of this result, the carrier recombination rate was researched with MASnBr₃ as the stacked structure and P₃HT as the HTL, as illustrated in Figure 4c,d. It can be clearly observed that when MASnBr₃ is the structure of the device, the carrier recombination rate of PSCs at 0–30 nm is 0 cm^{−3}s^{−1}, indicating that the device generates a good built-in electric field. However, when P₃HT is the structure of the device, the carrier recombination rate of PSCs at 0–30 nm reaches the highest, 1.59 × 10²¹ cm^{−3}s^{−1}, indicating that the electron transport inside the device deteriorates sharply, which degrades the performance of PSCs. In conclusion, MASnBr₃ is a suitable laminated structure material for titanium-based PSCs.

3.3. Influence of Defect Density in Laminated Structure PSCs

For PCSs, the ideal crystal structure of perovskite materials is that their atoms or organic groups are periodically arranged in their specific positions without the influence of foreign impurities. However, during the actual growth process, the material inevitably generates a large number of defects due to its soft ionic

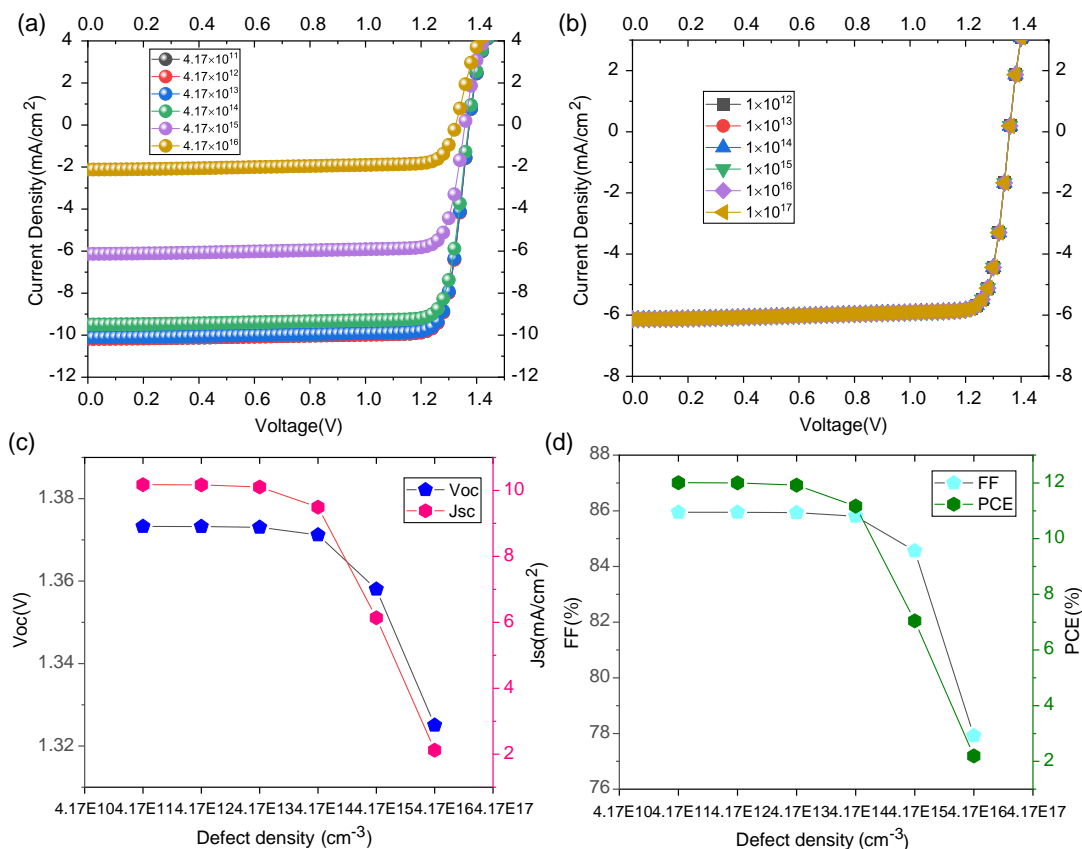


Figure 5. a) *J*–*V* of Cs₂TiBr₆ defect density variation and b) *J*–*V* of MASnBr₃ defect density variation. Changing Cs₂TiBr₆ defect density: c) V_{OC}, J_{SC}, d) FF, PCE.

properties, the volatile and low thermal stability of organic components, and the dislocation and fracture of the perovskite lattice at grain boundaries and surfaces. Therefore, the impact of defect density in the laminated structure PSCs on PSCs was explored. The defect density of the device absorber layer Cs_2TiBr_6 varied from 4.17×10^{11} to $4.17 \times 10^{16} \text{ cm}^{-3}$. The defect density of PSCs HTL MASnBr_3 was set to vary from 10^{12} to 10^{17} cm^{-3} . As displayed in Figure 5a, in order to adjust the $J-V$ curve of the defect density of Cs_2TiBr_6 , it can be found that in the low-doping-concentration region of 4.17×10^{11} – $4.17 \times 10^{13} \text{ cm}^{-3}$, the $J-V$ curves basically overlap, indicating that the optoelectronic properties of PSC changes are small. However, in the region of low doping concentration from 4.17×10^{14} to $4.17 \times 10^{16} \text{ cm}^{-3}$, the $J-V$ shifts significantly upward, indicating that the performance of PSCs deteriorates. The cause is that when the defect density of PSCs Cs_2TiBr_6 is too high, the carrier recombination rate will be greatly increased, and the whole performance of the device will be degraded. As shown in Figure 5b, in order to adjust the $J-V$ curve of the defect density of MASnBr_3 , it can be noted that the $J-V$ curve does not change whether MASnBr_3 is in the low-doping-concentration region or the high-doping-concentration region, indicating that the

absorption layer Cs_2TiBr_6 defect density dominates the effect of HTL MASnBr_3 on the properties of PSCs. Therefore, the effect of Cs_2TiBr_6 defect density on device performance parameters was further explored. As shown in Figure 5c, J_{SC} remains basically unchanged in the low-doping-concentration region. While in the high-doping-concentration region, the J_{SC} dropped significantly from 9.49% to 2.12%. As shown in Figure 4d, the performance parameters fill factor (FF) and PCE also show the same trend, which is also consistent with the results shown in Figure 5a. This may be due to the excessively high defect density, which causes the lifetime of the carriers to decay sharply, resulting in a decrease in the performance of the PCS.^[36] Based on the above analysis, and taking into account the level of the existing manufacturing process, the optimal values of defect densities of the Cs_2TiBr_6 and the MASnBr_3 are 4.17×10^{11} and 10^{15} cm^{-3} , respectively.

3.4. Influence of Laminated Structure PSCs' Thickness

The thickness of each layer in PSCs affects the generation and transport of carriers, which in return influences the performance

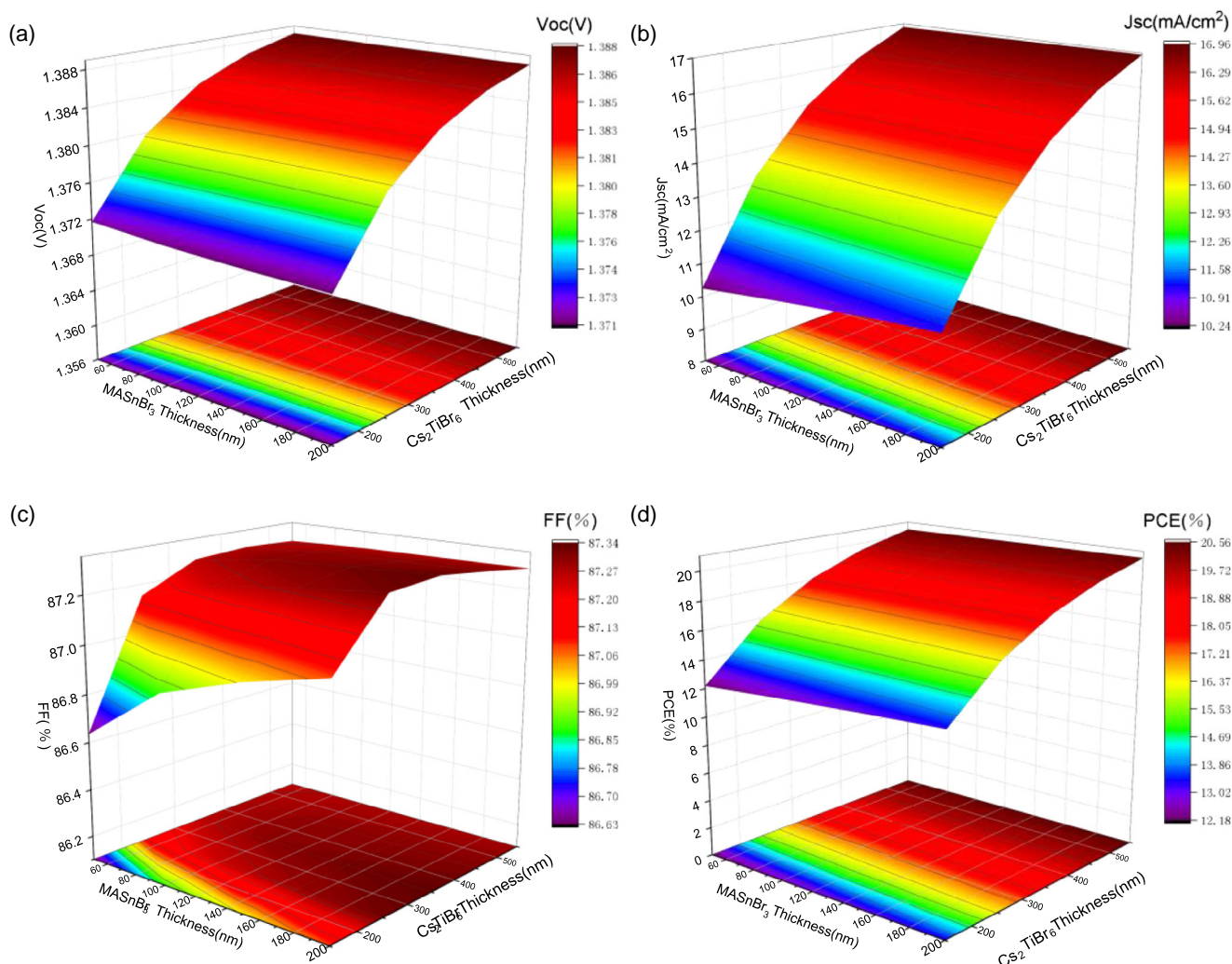


Figure 6. Change in the thickness of the absorber layer and HTL: a) V_{oc} , b) J_{sc} , c) FF, d) PCE.

of the device. Therefore, it is necessary to explore the effect of the thickness of the Cs_2TiBr_6 and the thickness of the HTL MASnBr_3 on PSCs. The variation interval of the thickness of Cs_2TiBr_6 is set between 150 and 550 nm, the variation interval of the thickness of MASnBr_3 is between 50 and 200 nm, and the performance parameters of the device are obtained. As shown in Figure 6a, it can be found that when the thickness of Cs_2TiBr_6 is between 150 and 350 nm, the V_{OC} increases from 1.37 to 1.38 V, and the rate of change slows down when Cs_2TiBr_6 exceeds 350 nm. Meanwhile, the thickness of Cs_2TiBr_6 dominates for V_{OC} . The changing trends of J_{SC} and PCE in Figure 6c,d are similar. As illustrated in Figure 6c, when the thickness of MASnBr_3 is between 50 and 100 nm, the variation of FF is larger, indicating that the stability of the device is degraded. Through the above analysis, it can be found that with the increase of the thickness of the laminated structure, the performance of PSCs increases significantly, but when the thickness of the absorbing layer is too high, the increase rate of various performance parameters is significantly slowed down. The cause is that as the thickness of the absorbing layer increases, enhanced light energy absorption of PSCs generates more photogenerated electrons and holes.^[37] Further addition of the absorber layer thickness would extend the carrier transport path and reduce the electric field within the absorber layer, resulting in compromised carrier transport within the device. Therefore, the thickness of the laminated structure is not easy to be too high, and 450 nm was finally selected as the optimum thicknesses of MASnBr_3 and Cs_2TiBr_6 , respectively.

3.5. Influence of Metal Electrodes and Temperature

Metal electrodes can have an important impact on the performance and stability of the device. We explored the effect of various metal electrodes on PSCs. The work functions of Ag, Cu, Fe, C, Au, and Ni were 4.57, 4.65, 4.81, 5, 5.1, and 5.5, respectively. As presented in Figure 7a, as the work function of the electrode increases, other performance parameters other than FF were significantly improved in the beginning, but when it reached Au

(5.1 eV), the changes in the performance parameters began to gradually slow down. As shown in Table 5, when the metal electrode was changed from Ag (4.57) to Au (5.1 eV), the work function difference was 0.53 eV, and the PCE of the device increased rapidly from 11.38% to 19.34%. When the metal electrode was changed from Au (5.1) to Ni (5.5 eV), the work function difference was 0.4 eV, and the PCE of the device did not change much, indicating that Au was the best metal electrode for the PSCs.

The operating temperature of PSCs is an application condition that cannot be ignored. In order to explore the performance of PSCs in harsh environments (high temperature, low temperature), the operating temperature of the device is set to vary from 230 to 430 K. As shown in Figure 7b, V_{OC} first increases and then decreases with increasing temperature, reaching a maximum value of 1.41 V at 270 K. The change of FF is just the opposite of V_{OC} . As the temperature increases, it first decreases and then increases, reaching a minimum value of 85.35% at 270 K. The higher FF reflects that the temperature has less influence on the stability of the device. At the same time, between 230 and 430 K, the variation range of PCE is between 17.83% and 19.63%. It is shown that the device can maintain high performance under a high-temperature or low-temperature working environment, which proves that the device has the properties of low-temperature and high-temperature resistance.

Table 5. The properties of different metal electrode devices.

Back metal	Ag	Cu	Fe	C	Au	Ni
Work function [eV]	4.57	4.65	4.81	5	5.1	5.5
V_{OC} [V]	0.95	1.03	1.19	1.36	1.38	1.38
J_{SC} [mA cm^{-2}]	16.22	16.22	16.22	16.22	16.22	16.23
FF [%]	73.93	75.68	78.54	81.93	87.31	90.24
PCE [%]	11.38	12.63	15.15	18.14	19.64	20.32

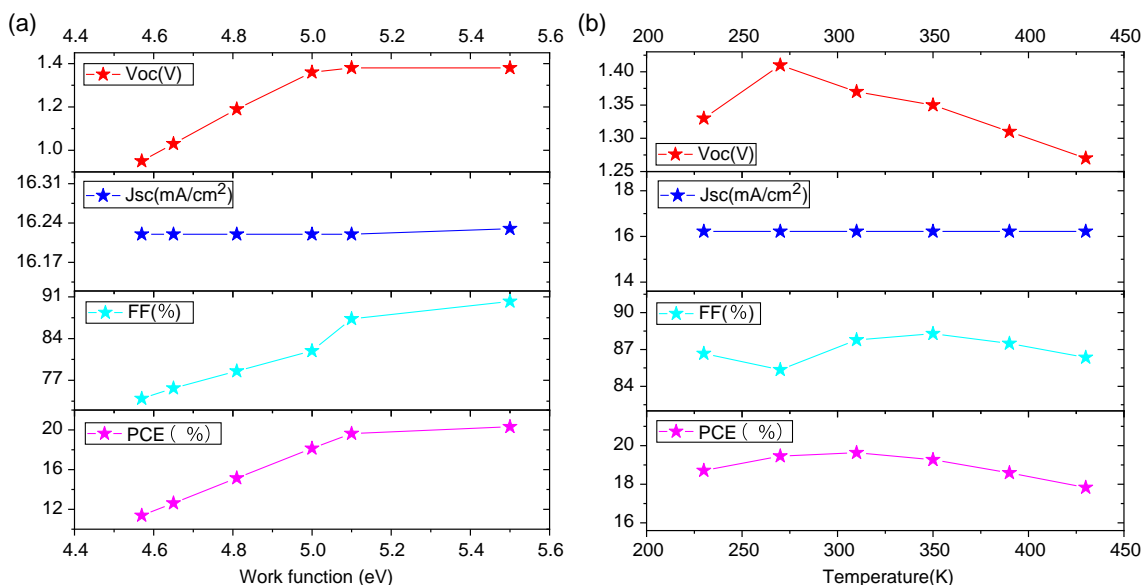


Figure 7. a) The effect of PSCs metal electrodes. b) The effect of operating temperature.

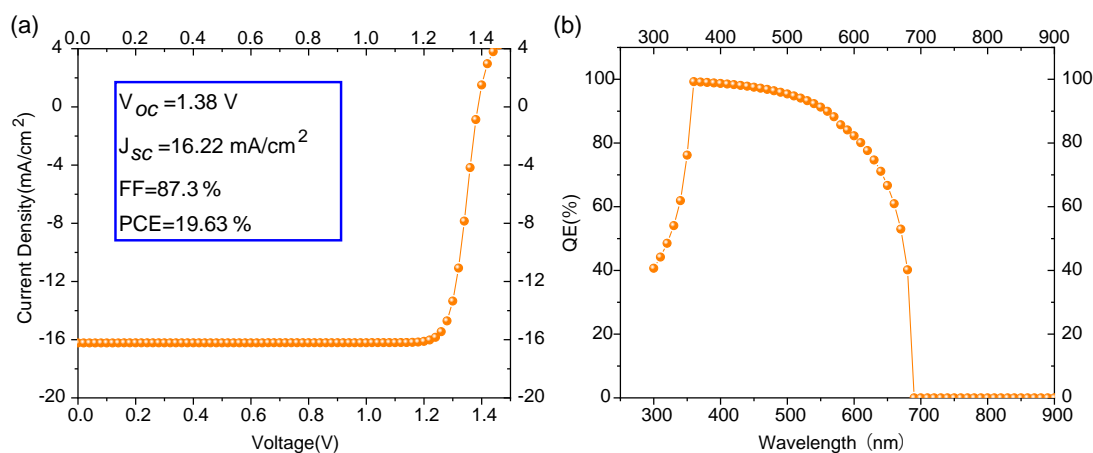


Figure 8. The performance of the final laminated structure: a) J - V and b) external QE.

Table 6. Performance comparison with other Ti-based PSCs.

Device Structure	V_{OC} [V]	J_{SC} [mA cm ⁻²]	FF [%]	PCE [%]	References
FTO/TiO ₂ /Cs ₂ TiBr ₆ /P ₃ HT/Au	0.89	3.87	59.5	2.15	[16]
FTO/TiO ₂ /C ₆₀ /Cs ₂ TiBr ₆ /P ₃ HT/Au	0.99	5.75	54.9	3.12	[16]
CuSCN/Cs ₂ TiBr ₆ /CdS/Si	8.9	—	—	6.68	[26]
FTO/TiO ₂ /Cs ₂ TiBr ₆ /NiO/Au	1.12	10.25	73.59	8.51	[38]
FTO/TiO ₂ /Cs ₂ TiBr ₆ /Cu ₂ O/Au	1.1	25.82	51.7	14.68	[39]
AZO/TiO ₂ /Cs ₂ TiBr ₆ /PEDOT: PSS/Au	1.38	18.2	71.0	17.83	[40]
FTO/SnO ₂ /Cs ₂ TiBr ₆ /MoO ₃ /Au	1.53	8.66	86.45	11.49	[28]
FTO/Cs ₂ TiBr ₆ /MASnBr ₃ /Au	1.38	16.22	87.3	19.63	this work

3.6. Final Optimization Results

Through the above analysis, the optimal materials and parameters of Ti-based PSCs were determined. MASnBr₃ was used as the HTL of the device. The defect density and thickness of the absorber layer Cs₂TiBr₆ are $4.17 \times 10^{11} \text{ cm}^{-3}$ and 450 nm, respectively. The defect density and thickness of MASnBr₃ are 10^{15} cm^{-3} and 150 nm, respectively. Au was used as the metal electrode for PSCs. After optimization, the J - V curve shown in Figure 8a and the QE curve shown in Figure 8b were obtained. It can be found that between 360 nm and 610 nm, the light energy utilization efficiency of PSCs is significantly improved, and the QE is above 80%. As shown in Table 6, for some recent reports of Ti-based PSCs, it can be found that the performance has also been significantly higher than the existing experiments and reports while reducing the cost of the device, which shows that the construction of the laminated structure is significant for the optoelectronic properties of PSCs.

4. Conclusion

In this study, a Cs₂TiBr₆/MASnBr₃ laminated PSC with no ETL structure was constructed and numerically simulated using

SCAPS-1D. The research results show that, in this structure, the ETL-free structure reduces the potential barrier between the interfaces, which improves the performance of the device. MASnBr₃ is used to replace the traditional HTL to form a laminated structure, which is more conducive to the built-in electric field of the PSCs. By researching the defect density and thickness, it is found that the defect density of Cs₂TiBr₆ has a dominant effect on the device performance, and the decrease of ETL thickness will reduce the stability of PSCs. By studying metal electrodes, it was found that Au with a work function of 5.1 eV is a suitable material. In order to explore the applicable environment of PSCs, the performance of PSCs in harsh environments (high temperature, low temperature) was explored. Studies have shown that the device maintains great operating levels between 230 and 430 K, proving that the PSCs are resistant to low and high temperatures. After optimization, the performance of PSCs is $V_{OC} = 1.38 \text{ V}$, $J_{SC} = 16.22 \text{ mA cm}^{-2}$, $FF = 87.3\%$, and $PCE = 19.63\%$. While using the ETL-free structure and laminated structure to reduce the device fabrication process and cost, it significantly improves the performance of PSCs. This work will provide a reference for realizing high-performance and low-cost ETL-free structure laminated PSCs in the future.

Supporting Information

Supporting Information is available from the Wiley Online Library or from the author.

Acknowledgements

L.Y. and X.Z. contributed equally to this work. This work was partially sponsored by National Natural Science Foundation of China (52076126), Shanghai Science and Technology Committee (22010501500), and Key Laboratory of Clean Power Generation and Environmental Protection Technology in Mechanical Industry.

Conflict of Interest

The authors declare no conflict of interest.

Data Availability Statement

The data that support the findings of this study are available from the corresponding author upon reasonable request.

Keywords

Cs₂TiBr₆, electron transport layer free, laminated structures, SCAPS-1D., Ti-based perovskite solar cells

Received: January 31, 2023
Revised: March 23, 2023
Published online: June 19, 2023

- [1] F. Wang, T. Tang, R. Zhang, Z. Cheng, J. Wu, P. He, Y. Qi, S. Chen, W. Li, *Fuel* **2022**, 326, 125117.
- [2] L. Chen, C. Li, Y. Zhao, J. Wu, X. Li, Z. Qiao, P. He, X. Qi, Z. Liu, G. Wei, *Chem. Eng. J.* **2021**, 425, 131599.
- [3] A. Kojima, K. Teshima, Y. Shirai, T. Miyasaka, *J. Am. Chem. Soc.* **2009**, 131, 6050.
- [4] A. Hima, N. Lakhdar, *Opt. Mater.* **2020**, 99, 109607.
- [5] B. Conings, J. Drijkoningen, N. Gauquelin, A. Babayigit, J. D'Haen, L. D'Olieslaeger, A. Ethirajan, J. Verbeeck, J. Manca, E. Mosconi, F. D. Angelis, H.-G. Boyen, *Adv. Mater.* **2015**, 5, 1500477.
- [6] L. Dou, Y. M. Yang, J. You, Z. Hong, W. H. Chang, G. Li, Y. Yang, *Nat. Commun.* **2014**, 5, 5404.
- [7] D. Han, M. Imran, M. Zhang, S. Chang, X. G. Wu, X. Zhang, J. Tang, M. Wang, S. Ali, X. Li, G. Yu, J. Han, L. Wang, B. Zou, H. Zhong, *ACS Nano* **2018**, 12, 8808.
- [8] M. M. Lee, J. Teuscher, T. Miyasaka, T. N. Murakami, H. J. Snaith, *Science* **2012**, 338, 643.
- [9] H. Zhu, Y. Fu, F. Meng, X. Wu, Z. Gong, Q. Ding, M. V. Gustafsson, M. T. Trinh, S. Jin, X. Y. Zhu, *Nat. Mater.* **2015**, 14, 636.
- [10] G. Flora, D. Gupta, A. Tiwari, *Interdiscip. Toxicol.* **2012**, 5, 47.
- [11] F. Giustino, H. J. Snaith, *ACS Energy Lett.* **2016**, 1, 1233.
- [12] M. H. Kumar, S. Dharani, W. L. Leong, P. P. Boix, R. R. Prabhakar, T. Baikie, C. Shi, H. Ding, R. Ramesh, M. Asta, M. Graetzel, S. G. Mhaisalkar, N. Mathews, *Adv. Mater.* **2014**, 26, 7122.
- [13] M. E. Kayesh, K. Matsuiishi, R. Kaneko, S. Kazaoui, J. J. Lee, T. Noda, A. Islam, *ACS Energy Lett.* **2019**, 4, 278.
- [14] A. Raj, M. Kumar, A. Anshul, *Phys. Status Solidi A* **2022**, 219, 2200425.
- [15] A. H. Slavney, T. Hu, A. M. Lindenberg, H. I. Karunadasa, *J. Am. Chem. Soc.* **2016**, 138, 2138.
- [16] M. Chen, M.-G. Ju, A. D. Carl, Y. Zong, R. L. Grimm, J. Gu, X. C. Zeng, Y. Zhou, N. P. Padture, *Joule* **2018**, 2, 558.
- [17] E. Mosconi, P. Umari, F. De Angelis, *Phys. Chem. Chem. Phys.* **2016**, 18, 27158.
- [18] M.-G. Ju, M. Chen, Y. Zhou, H. F. Garces, J. Dai, L. Ma, N. P. Padture, X. C. Zeng, *ACS Energy Lett.* **2018**, 3, 297.
- [19] D. Kong, D. Cheng, X. Wang, K. Zhang, H. Wang, K. Liu, H. Li, X. Sheng, L. Yin, *J. Mater. Chem. C* **2020**, 8, 1591.
- [20] X. Yang, Q. Li, Y. Zheng, D. Luo, Y. Zhang, Y. Tu, L. Zhao, Y. Wang, F. Xu, Q. Gong, *Joule* **2022**, 6, 1277.
- [21] B. He, L. Liu, J. Hu, S. Nie, Y. Chen, Y. Chen, *J. Phys. D: Appl. Phys.* **2022**, 55, 015107.
- [22] L. Hao, X. Wu, H. Wang, Y. Song, X. Ma, Z. Zeng, J. Wu, Y. Tao, Z. Wang, Y. Liu, *Opt. Quantum Electron.* **2022**, 54, 1.
- [23] M. Burgelman, P. Nollet, S. Degraeve, *Thin Solid Films* **2000**, 361, 527.
- [24] M. Kumar, A. Kumar, A. Raj, P. C. Sati, M. Sahni, A. Anshul, *Mater. Today Proc.* **2022**, 49, 3081.
- [25] A. Raj, M. Kumar, A. Kumar, Z. R. Khan, A. Anshul, *Macromol. Symp.* **2023**, 407, 2100482.
- [26] K. Chakraborty, M. G. Choudhury, S. Paul, *Sol. Energy* **2019**, 194, 886.
- [27] S. A. Moiz, A. N. M. Alahmadi, *Polymers* **2021**, 13, 2110.
- [28] S. Ahmed, F. Jannat, M. A. K. Khan, M. A. Alim, *Optik* **2021**, 225, 165765.
- [29] S. A. Moiz, *Photonics* **2021**, 9, 23.
- [30] A. Raj, M. Kumar, H. Bherwani, A. Gupta, A. Anshul, *J. Vac. Sci. Technol., B: Nanotechnol. Microelectron.: Mater., Process., Meas., Phenom.* **2021**, 39, 012401.
- [31] S. Abdelaziz, A. Zekry, A. Shaker, M. Abouelatta, *Opt. Mater.* **2020**, 101, 109738.
- [32] P. K. Patel, *Sci. Rep.* **2021**, 11, 1.
- [33] J. M. Ball, M. M. Lee, A. Hey, H. J. Snaith, *Energy Environ. Sci.* **2013**, 6, 1739.
- [34] B. Farhadi, M. Ciprian, F. Zabihi, A. Liu, *Sol. Energy* **2021**, 226, 161.
- [35] K. Deepthi Jayan, V. Sebastian, *Sol. Energy* **2021**, 217, 40.
- [36] X. Li, J. Li, S. Wu, Y. Li, C. Peng, M. Wu, J. Wu, J. Lin, X. Ma, S. Huang, *Sol. Energy* **2022**, 247, 315.
- [37] Z. Qiao, M. Zhang, B. Wu, T. Zhang, Y. Ruan, J. Chen, L. Huang, J. Wu, Y. Qi, X. Yang, *Chem. Phys. Lett.* **2023**, 813, 140295.
- [38] M. Samanta, S. I. Ahmed, K. K. Chattopadhyay, C. Bose, *Optik* **2020**, 217, 164805.
- [39] M. R. Jani, M. T. Islam, S. M. Al Amin, M. S. U. Sami, K. M. Shorowordi, M. I. Hossain, *Superlattices Microstruct.* **2020**, 146, 106652.
- [40] S. A. Moiz, A. N. M. Alahmadi, A. J. Aljohani, *IEEE Access* **2021**, 9, 54254.